Multi-level cognitive control and terrain adaptive quadruped robot simulation in MATLAB

Prem Sankar N[1,2,*], *Sidharth* P J[2], *Harish* T[2], and *Nanthan* S Nair[2]

[1] Centre for Healthcare Advancement, Innovation and Research, Vellore Institute of Technology, Chennai, India
[2] School of Computer Science and Engineering, Vellore Institute of Technology, Chennai, India

Abstract. Legged robots, particularly quadrupeds, have emerged as an essential research focus for traversing unstructured environments where wheeled systems are limited. This paper presents a novel Multi-Level Cognitive Control Architecture (MLCCA) for a quadruped robot, inspired by biological hierarchical intelligence. The primary novelty of this work lies in the integration of three bio-inspired cognitive layers—a fast reactive layer (Microscopic Brain), a mid-level adaptive layer (Mesoscopic Brain), and a high-level strategic planner (Macroscopic Brain)—into a unified, mathematically formalized control framework implemented entirely in MATLAB without requiring deep learning or extensive hardware. Unlike prior approaches that address either reflexive or deliberative control in isolation, the proposed architecture simultaneously handles immediate obstacle avoidance, terrain-adaptive gait modulation, and long-term path planning within a single coherent system. The robot dynamically alters its gait parameters based on local terrain gradients and obstacle height using height interpolation and cognitive decision rules. The simulation integrates procedural terrain generation and wireframe-based gait control visualization. Results demonstrate successful traversal of unpredictable terrain with intelligent gait adaptation and obstacle avoidance, achieving a mean body tilt of only 0.075rad and a path efficiency ratio of 1.18. This framework provides a scalable foundation for cognitive robotics, integrating perception, reflex, and long-term strategy into a unified control system.

1 Introduction

The domain of legged robotics has evolved significantly over the past decade, driven by the need for autonomous systems capable of traversing unstructured, uneven, and unpredictable terrains.

* Corresponding author: premsankar.n@vit.ac.in

.

Unlike wheeled or tracked vehicles, legged robots can maintain stability and locomotion efficiency across diverse ground profiles, making them highly suitable for applications such as planetary exploration, disaster response, and military reconnaissance. Among legged morphologies, quadrupeds strike an effective balance between mechanical stability and maneuverability, closely mimicking the biological locomotion mechanisms found in mammals.

Despite recent advancements, the majority of quadruped control systems remain limited by rigid control hierarchies and linear decision models. Traditional approaches employ predefined gait cycles and trajectory planners that function effectively on flat terrain but fail to adapt dynamically to environmental variations. Moreover, most robotic architectures rely on a single-layer control paradigm, resulting in delayed reflexes, inefficient obstacle handling, and limited situational awareness. These limitations underline the need for a more intelligent, multi-layered cognitive model that integrates both reflexive and deliberative behaviors.

Inspired by cognitive neuroscience and hierarchical control theory, this work proposes a Multi-Level Cognitive Control Architecture (MLCCA) for terrain-adaptive quadruped locomotion. The design introduces three cognitive layers operating at different temporal and spatial resolutions: a Microscopic Brain for fast reflexive reactions, a Mesoscopic Brain for mid-level environmental awareness and local decision-making, and a Macroscopic Brain for long-term strategic planning and path optimization. Each layer operates semi-independently yet contributes to a unified behavioral output, analogous to multi-scale cognitive processing in biological organisms.

1.1 Motivation and background

The development of intelligent mobile robots capable of autonomous navigation in complex environments has been a longstanding goal in robotics research. Biological systems, particularly mammals, exhibit remarkable capabilities in locomotion across diverse terrains through the integration of multiple neural processing layers. The human nervous system, for instance, processes sensory information at different hierarchical levels: spinal reflexes provide immediate responses to stimuli, the cerebellum coordinates movement and balance, and the cerebral cortex handles high-level planning and decision-making.

This biological inspiration forms the foundation of the proposed multi-level cognitive architecture. By emulating the hierarchical structure of biological intelligence, the aim is to create a robotic control system that exhibits both reactive and deliberative behaviors, enabling robust performance in unpredictable environments. The proposed architecture addresses several critical challenges in quadruped robotics:

- **Real-time responsiveness**: The microscopic layer ensures immediate reactions to sudden obstacles or terrain changes, mimicking spinal reflex arcs.
- **Adaptive gait modulation**: The mesoscopic layer adjusts locomotion parameters based on terrain characteristics, analogous to cerebellar function.
- **Strategic navigation**: The macroscopic layer plans optimal paths and makes high-level decisions, analogous to cortical processing.

1.2 Novelty and key contributions

The principal novelty of this work is threefold. First, a unified three-layer cognitive control architecture is proposed wherein the reflexive, adaptive, and strategic layers operate at explicitly defined timescales (100Hz, 20Hz, and 2Hz, respectively) and communicate through a shared blackboard mechanism, eliminating the latency issues that

arise in sequential architectures. Second, a rigorous mathematical formulation unifies the contributions of all three layers into a single control signal, enabling transparent analysis of inter-layer dynamics. Third, the entire system—including procedural terrain generation, sensor simulation, inverse kinematics, and real-time 3D visualization—is realized in MATLAB without reliance on external physics engines or deep learning, demonstrating that biologically inspired cognitive control can achieve strong performance with transparent, interpretable algorithms. The main contributions of this work are:

- A novel multi-level cognitive control architecture for quadruped robots inspired by biological hierarchical intelligence.
- Mathematical formulation of control signals across three cognitive layers with explicit integration and symbol definitions.
- A complete MATLAB implementation with procedural terrain generation and real-time visualization.
- Comprehensive evaluation using stability, control accuracy, sensitivity, and behavioral metrics.
- Quantitative demonstration of terrain-adaptive locomotion in simulation, outperforming single-layer and two-layer alternatives.

1.3 Paper organization

The remainder of this paper is structured as follows. Section 2 reviews the existing literature on quadruped locomotion and cognitive robotic control systems. Section 3 details the methodology and architecture of the proposed multi-level brain model. Section 4 presents the experimental setup and implementation details. Section 5 discusses the results and performance analysis. Section 6 concludes with potential directions for future research.

2 Literature review

Quadruped robots have been a major focus of research due to their superior mobility in unstructured environments compared to wheeled or tracked platforms. This section reviews the state of the art in quadruped locomotion, hierarchical control systems, and biologically inspired robotics.

2.1 Evolution of quadruped robotics

Early efforts in dynamic quadruped locomotion focused on hardware design and trajectory control for stable walking and running. Bledt et al. introduced the MIT Cheetah 3, demonstrating dynamic rough-terrain traversal using high-bandwidth proprioceptive actuators and a modular control architecture that handles unexpected terrain disturbances without exteroceptive sensing [2]. This work established a benchmark hardware platform that influenced subsequent generations of quadruped robots and inspired a broad research programme in dynamic legged locomotion.

Bellicoso et al. extended this foundation by developing whole-body control frameworks for the ANYmal quadruped, coupling task-space controllers with dynamic gait generation to achieve stable locomotion and transitions across a variety of terrain conditions [7]. Their hierarchical structure decomposed the control problem into multiple layers, each responsible for specific aspects of locomotion, improving computational efficiency and enabling real-time performance. Similarly, Bellicoso et al. demonstrated online trajectory

optimisation strategies allowing quadrupeds to adapt to unpredictable terrain in real time [9], emphasising the importance of combining reactive control with predictive planning, a principle that aligns closely with the multi-level cognitive architecture proposed in the present work.

2.2 Control strategies and hierarchical approaches

Control strategies have evolved from single-layer reflexive controllers to sophisticated hierarchical and biologically inspired approaches. Sleiman et al. proposed a unified Model Predictive Control (MPC) framework incorporating whole-body dynamics for simultaneous locomotion and manipulation, demonstrating that integrating multiple control layers significantly improves dynamic performance compared to decoupled joint-level controllers [1]. Their work highlighted that coordinated whole-body control is essential for achieving both stability and agility in complex tasks.

Hwangbo et al. explored reinforcement-learning-based motor skill acquisition for legged robots, emphasising the benefits of adaptive gait generation discovered through simulation-to-real transfer [3]. Machine learning approaches have shown considerable promise in discovering optimal control policies through environment interaction, though they typically require extensive training and may lack interpretability in safety-critical scenarios.

Hierarchical cognitive control frameworks, as discussed by Li et al., provide an effective approach for integrating fast reflexive responses, short-term terrain memory, and long-term planning, directly aligning with the methodology presented in this work [6]. Di Carlo et al. further demonstrated that convex MPC with a simplified rigid-body dynamics model can compute optimal ground reaction forces in under 1 ms, enabling real-time, multi-gait locomotion at high speeds [10]. More recently, Agrawal et al. showed that hierarchical MPC can achieve agile locomotion on challenging terrain with minimal parameter tuning [18].

2.3 Terrain adaptation and environmental awareness

Terrain adaptation remains a critical aspect of quadruped locomotion. Mastalli et al. developed a coupled framework for motion planning, terrain mapping, and whole-body control that enables quadrupeds to select safe footholds and optimise body trajectories online without a pre-built map [11]. Their approach demonstrated that simultaneously solving the planning and control problem produces significantly more robust outdoor locomotion than sequential decoupled solutions.

Miki et al. extended terrain-adaptive locomotion to fully perceptive scenarios, training a controller that fuses proprioceptive history with exteroceptive height maps through an attention-based recurrent encoder [8]. Deployed on natural Alpine terrain, their system achieved locomotion robustness that surpassed manually engineered model-based controllers in uncontrolled conditions. Control accuracy and stability metrics, including tilt magnitude, foot clearance, and body orientation, have been widely used to evaluate performance across these approaches [12, 15]. Grimminger et al. provided a comprehensive open-source hardware and software platform for quadrupedal locomotion research,

establishing standardised stability evaluation tools and metrics for the community [12]. Recent work by Zhuang et al. introduced extreme agility on complex terrain through end-to-end vision-based parkour learning, further extending terrain-adaptation capabilities to obstacle climbing, gap leaping, and crawling under barriers [22].

2.4 Biologically inspired control models

Biologically inspired control models have strongly influenced modern robot locomotion research. Saveriano et al. provided a comprehensive tutorial survey on Dynamic Movement Primitives (DMPs), which encode motor skills as stable dynamical systems that can be generalised to new targets, combined modularly, and adapted to perturbations, making them well suited for encoding locomotion primitives in legged robots [14]. Their work systematically catalogues discrete, periodic, and Cartesian-space DMP formulations, covering the full scope of applications relevant to gait generation and recovery behaviours.

Kong et al. applied DMPs to robot skill learning from demonstrations, integrating Gaussian Mixture Models to extract richer motion features and an adaptive neural network controller to ensure accurate tracking of DMP-generated reference trajectories [16]. Their system demonstrated that demonstration-based skill learning can be reliably transferred to physical robotic systems, providing a practical pathway from motion capture data to deployable locomotion skills.

Gupta et al. emphasised the interaction between body morphology and cognitive control in achieving intelligent behaviour, demonstrating through neuro-evolution combined with deep reinforcement learning that embodied intelligence, where morphology and controller co-evolve, produces agents qualitatively superior to those optimised through control alone [13]. Their findings support the concept of multi-level cognitive architectures in which the physical body is an active participant in computation rather than a passive substrate. Passive-dynamic and energy-efficient gait models [17] also provide complementary insights into how appropriate mechanical design can reduce control demands and improve energy efficiency, as further formalised by Khadiv et al. who demonstrated that adaptive step timing, adjusting both when and where footfalls occur, dramatically improves robustness to large disturbances compared to fixed-timing controllers [17]. More recently, Shi et al. demonstrated CPG-based locomotion with online adaptation for quadrupeds navigating unfamiliar terrain, achieving superior energy efficiency compared to pure model-predictive approaches [21].

2.5 Sensing and perception

Recent advances integrate multi-sensory feedback, mapping, and perception for robust navigation. Bavle et al. surveyed the progression from Simultaneous Localisation and Mapping (SLAM) toward full situational awareness, distinguishing metric, metric–semantic, and topological scene representations that are critical for the mesoscopic and macroscopic cognitive layers of a hierarchical controller [18]. Their taxonomy provides a principled framework for selecting appropriate perception representations depending on the temporal and spatial scale of the locomotion task.

Hwang and Hodgins highlighted the integration of proprioceptive sensing with reflexive feedback loops to enhance locomotion in unpredictable environments, demonstrating that biologically motivated hierarchical sensing, separating fast spinal-level reflexes from slower cognitive processing, produces measurably more robust walking [4]. Li et al. further showed that hierarchical cognitive architectures that fuse LiDAR, vision, and proprioception across three distinct temporal layers enable robots to maintain safe locomotion in dynamically changing outdoor environments [6]. Additionally, modern quadrupeds increasingly employ predictive and learning-based approaches to balance stability, energy efficiency, and real-time responsiveness across variable conditions [3, 5].

2.6 Summary and research gap

In summary, the literature establishes that hierarchical, multi-level cognitive models inspired by biological systems provide significant advantages for quadruped locomotion in rough and unpredictable terrains. Reflexive fast responses, mid-level terrain adaptation, and high-level planning together allow robots to navigate complex environments while maintaining stability and control accuracy. The convergence of model-based MPC frameworks [1, 10, 11], reinforcement learning [3, 8, 17], and biologically grounded skill representations [14, 16, 21] has produced systems of unprecedented capability, demonstrated in field deployments ranging from subterranean exploration to alpine hiking and urban parkour [8, 22].

However, most existing approaches focus on either low-level control or high-level planning, with limited principled integration between layers. Furthermore, many systems require extensive training pipelines, large sensor suites, or high computational budgets, limiting their applicability in resource-constrained scenarios. The present study builds on these findings by implementing a multi-layer brain architecture that integrates microscopic, mesoscopic, and macroscopic control layers for robust simulation-based quadruped locomotion, with explicit mathematical formulation and efficient implementation in MATLAB.

3 Methodology

3.1 Overview of the proposed model

The proposed system introduces a Multi-Level Smart Robot Brain (MLSRB), a bio-inspired hierarchical control model that emulates the layered structure of the human nervous system. It comprises three interconnected intelligence modules, each operating at different temporal and spatial scales. Table 1 summarizes the three cognitive layers, their corresponding biological analogies, operating frequencies, inputs, processing mechanisms, and outputs. The three layers are detailed below:

Table 1. Summary of the three cognitive layers: inputs, processing, and outputs

Layer	Inputs	Processing	Outputs
Microscopic (Spinal Reflex, 100–200Hz)	Obstacle distance d_{obs}, foot contact forces	Threshold comparison, immediate threat assessment	Emergency correction signals
Mesoscopic (Cerebellum, 20–50Hz)	Terrain gradient ∇h, body tilt θ, recent gait history	Gait parameter adjustment, balance control, short-term prediction	Modified gait parameters (step height, stride, freq.)
Macroscopic (Cortex, 1–10Hz)	Global terrain map, goal location, current position	Path planning, energy optimization, mission objectives	Desired velocity, heading

- **Microscopic (Fast) Brain**: A reflexive controller responding to immediate stimuli. Analogous to the human spinal cord reflex arc, this layer operates at the highest frequency (100–200Hz) and provides immediate responses to sudden obstacles or terrain changes. The microscopic brain relies on simple threshold-based rules and does not require extensive computation.
- **Mesoscopic (Medium) Brain**: An adaptive controller that builds a short-term memory of terrain features and gait corrections. Comparable to the cerebellum's role in balance and coordination, this layer operates at moderate frequency (20–50Hz) and adjusts gait parameters based on local terrain characteristics. It maintains a sliding window of recent sensory data to detect trends and patterns.
- **Macroscopic (Slow) Brain**: A strategic planner that maps environment layouts, optimizes paths, and makes long-term locomotion decisions. Functionally equivalent to the cerebral cortex, this layer operates at lower frequency (1–10Hz) and handles global navigation, path planning, and mission-level objectives.

Each level operates asynchronously but communicates via a shared blackboard architecture. Sensory data (from ultrasonic, IMU, or simulated terrain sensors) are interpreted at different temporal scales, ensuring both real-time reflexes and long-horizon planning.

3.2 System architecture

The system architecture integrates perception, cognition, and motor control units across three layers. The architecture follows a hierarchical organization in which higher-level layers set goals and constraints for lower-level layers, while lower-level layers provide feedback and request assistance when necessary. Figure 1 illustrates the complete multi-level cognitive control architecture, showing how perception inputs flow through the three cognitive layers to the motor control system and eventually interact with the physical environment.

3.2.1 Percept

ion module

The perception module processes raw sensory data and extracts relevant features for each cognitive layer:

- **Proprioceptive sensing**: Joint encoders, IMU data (acceleration, angular velocity, orientation).
- **Exteroceptive sensing**: Ultrasonic rangefinders, terrain height sensors (simulated), contact sensors.
- **Feature extraction**: Obstacle detection, terrain gradient estimation, body orientation, foot contact states.

3.2.2 Cognition module

The cognition module consists of three sub-modules corresponding to the three brain layers:

1. **Microscopic cognition**: Reflex controller.
   - *Input*: Obstacle proximity d_{obs}, foot contact forces.
   - *Processing*: Threshold comparison, immediate threat assessment.
   - *Output*: Emergency correction signals $\mathbf{u}_{\text{micro}}$.
2. **Mesoscopic cognition**: Adaptive controller.
   - *Input*: Terrain gradient ∇h, body tilt θ, recent gait history.
   - *Processing*: Gait parameter adjustment, balance control, short-term prediction.
   - *Output*: Modified gait parameters—stride length l_{stride}, step height h_{step}, gait frequency f_{gait}.
3. **Macroscopic cognition**: Strategic planner.
   - *Input*: Global terrain map, goal location $\mathbf{p}_{\text{goal}}$, current position $\mathbf{p}$.
   - *Processing*: Path planning via potential fields, energy optimization, mission objectives.
   - *Output*: Desired velocity, heading, and behavioral mode selection.

3.2.3 Motor Control Module

The motor control module translates high-level commands into joint-level actuator commands:

- Inverse kinematics: Computes joint angles for desired foot positions (see Section 3.5.2).
- Trajectory generation: Produces smooth foot trajectories during the swing phase.
- Torque control: Implements desired forces and impedances at the joints.
- Gait coordination: Synchronizes leg movements according to the selected gait pattern.

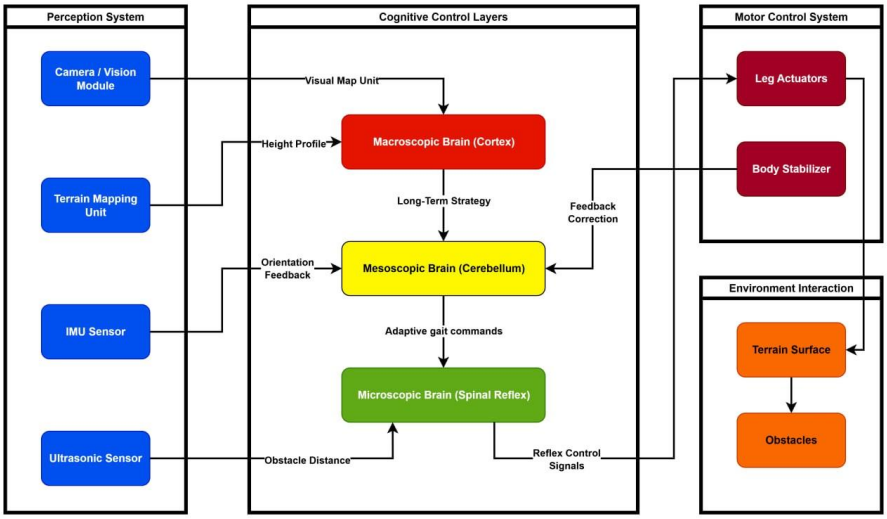

Fig. 1 Multi-level cognitive control architecture of the proposed system.

The architecture comprises three tiers: (i) a *Perception Layer* including Camera/Vision Module, Terrain Mapping Unit, IMU Sensor, and Ultrasonic Sensor that acquire environmental data; (ii) a *Cognitive Control Layer* with the Macroscopic Brain (Cortex) for long-term strategy, the Mesoscopic Brain (Cerebellum) for adaptive gait commands, and the Microscopic Brain (Spinal Reflex) for immediate responses; and (iii) a *Motor Control Layer* consisting of Leg Actuators and Body Stabilizer that execute commands. Arrows indicate the direction of information flow from sensing through cognition to actuation and back via feedback loops. The three cognitive layers operate at 1–10Hz, 20–50Hz, and 100–200Hz, respectively.

3.3 Mathematical modeling

3.3.1 State representation

Let the state vector of the robot be defined as:

$$\mathbf{x}(t) = [p_x,\ p_y,\ p_z,\ \theta_x,\ \theta_y,\ \theta_z]^T \tag{1}$$

where $\mathbf{p} = [p_x, p_y, p_z]^T \in \mathrm{R}^3$ denotes the position of the robot body in the world frame, and $\theta = [\theta_x, \theta_y, \theta_z]^T$ denotes the orientation (roll, pitch, and yaw angles, respectively).

The complete state also includes velocities and joint configurations:

$$\mathbf{X}(t) = [\mathbf{x}(t)^T,\ \dot{\mathbf{x}}(t)^T,\ \mathbf{q}(t)^T,\ \dot{\mathbf{q}}(t)^T]^T \tag{2}$$

where $\mathbf{q}(t) \in \mathrm{R}^8$ represents the joint angles of the four legs (two degrees of freedom per leg), and $\dot{\mathbf{q}}(t) \in \mathrm{R}^8$ denotes their angular velocities.

3.3.2 Multi-level control formulation

The total control input $\mathbf{u}(t)$ is the superposition of contributions from each cognitive layer:

$$\mathbf{u}(t) = \mathbf{u}\text{micro}(t) + \mathbf{u}\text{meso}(t) + \mathbf{u}\text{macro}(t) \quad (3)$$

where $\mathbf{u}_{\text{micro}}$, $\mathbf{u}_{\text{meso}}$, and $\mathbf{u}_{\text{macro}}$ are the control vectors from the microscopic, mesoscopic, and macroscopic layers, respectively. Their sum forms the total actuator command applied to the robot.

3.3.3 Microscopic layer: reflexive control

The microscopic brain generates a reflexive repulsive control signal activated when the distance to an obstacle d_{obs} falls below a safety threshold d_{safe}:

$$\mathbf{u}\text{micro}(t) = Kr\,(d\text{obs} - d\text{safe})+ \mathbf{n}\hat{}\text{obs} \quad (4)$$

where:

- $K_r > 0$ is the reflexive gain coefficient (units: N/m),
- d_{obs} is the measured distance to the nearest obstacle (m),
- d_{safe} is the safety distance threshold (m); the robot is safe when $d_{\text{obs}} \geq d_{\text{safe}}$,
- $(x)^+ = \max(0,-x)$ is a ramp function that ensures the control is active only when $d$obs < $d$safe,
- $\mathbf{n}\hat{}_{\text{obs}} \in \mathrm{R}^3$ is the unit vector pointing away from the obstacle (repulsion direction).

This control law produces a repulsive force proportional to obstacle proximity, providing immediate collision avoidance.

3.3.4 Mesoscopic layer: adaptive terrain control

The mesoscopic brain generates adaptive terrain control signals proportional to the local terrain gradient $\nabla h(\mathbf{p})$:

$$\mathbf{u}_{\text{meso}}(t) = K_a \nabla h(\mathbf{p}) + K_b(\theta_{\text{des}} - \theta_{\text{actual}}) \quad (5)$$

where:

- $K_a > 0$ is the terrain adaptation gain (dimensionless),
- $\nabla h(\mathbf{p}) \in \mathrm{R}^2$ is the local terrain height gradient evaluated at robot position $\mathbf{p}$,
- $K_b > 0$ is the posture correction gain (units: N·m/rad),
- θ_{des} is the desired body orientation vector (rad), – θ_{actual} is the measured body orientation from the IMU (rad).

Additionally, the mesoscopic layer modulates gait parameters as follows:

$$\begin{aligned} \text{Step height:} \quad & h_{\text{step}}(t) = h_0 + \alpha\|\nabla h(\mathbf{p})\| \\ \text{Stride length:} \quad & l_{\text{stride}}(t) = l_0 - \beta\|\nabla h(\mathbf{p})\| \\ \text{Gait frequency:} \quad & f_{\text{gait}}(t) = f_0 - \gamma\|\nabla h(\mathbf{p})\| \end{aligned} \quad (6)$$

where h_0, l_0, f_0 are the nominal step height (m), stride length (m), and gait frequency (Hz), respectively; and α (m), β (m), γ (Hz) are terrain-adaptation coefficients that scale the response to terrain gradient magnitude $\|\nabla h(\mathbf{p})\|$.

3.3.5 Macroscopic Layer: Strategic Planning

The macroscopic brain employs a potential field-based navigation strategy:

$$\mathbf{u}_{\text{macro}}(t) = -\nabla V(\mathbf{p}) \tag{7}$$

where $V(\mathbf{p})$ is a composite potential field combining attractive and repulsive components:

$$V(\mathbf{p}) = V_{\text{att}}(\mathbf{p}) + \sum_i V_{\text{rep},i}(\mathbf{p}) \tag{8}$$

The attractive potential draws the robot toward the goal:

$$V_{\text{att}}(\mathbf{p}) = \frac{1}{2} k_{\text{att}} \|\mathbf{p} - \mathbf{p}_{\text{goal}}\|^2 \tag{9}$$

where $k_{\text{att}} > 0$ (dimensionless) is the attractive gain and $\mathbf{p}_{\text{goal}}$ is the goal position (m).

The repulsive potential for the i-th known obstacle is defined as:

$$V_{\text{rep},i}(\mathbf{p}) = \begin{cases} \frac{1}{2} k_{\text{rep}} \left(\frac{1}{d_i} - \frac{1}{d_0} \right)^2 & \text{if } d_i \le d_0 \\ 0 & \text{if } d_i > d_0 \end{cases} \tag{10}$$

where $d_i = \|\mathbf{p} - \mathbf{p}_{\text{obs},i}\|$ is the Euclidean distance to obstacle i (m), d_0 is the repulsion influence radius (m), and $k_{\text{rep}} > 0$ is the repulsive gain (dimensionless).

3.3.6 System dynamics

The resulting motion dynamics are expressed as:

$$\dot{\mathbf{x}} = f(\mathbf{x}) + g(\mathbf{x})\mathbf{u}(t) \tag{11}$$

where $f(\mathbf{x})$ denotes the passive body dynamics (drift term) and $g(\mathbf{x})$ is the actuator influence matrix (control effectiveness). For the simulated quadruped, the translational dynamics are approximated as:

$$\dot{p}_x = v_x,\ \dot{p}_y = v_y,\ \dot{p}_z = v_z \quad m\dot{v}_x = F_x - c_x v_x \tag{12}$$
$$m\dot{v}_y = F_y - c_y v_y \quad m\dot{v}_z = F_z - mg - c_z v_z$$

where m (kg) is the robot mass;
F_x, F_y, F_z (N) are the control forces from $\mathbf{u}(t)$;
c_x, c_y, c_z (N·s/m) are velocity-damping coefficients;
and $g = 9.81 \text{m/s}^2$ is gravitational acceleration

3.4 Terrain modeling

The simulated environment consists of a procedurally generated terrain with randomly distributed obstacles. The terrain height function is:

$$z(x,y) = A\sin(kx)\cos(ky) + \sum_i \gamma_i \exp\left(-\frac{\left\|[x,y]^T - [x_i,y_i]^T\right\|^2}{\sigma_i^2}\right) \quad (13)$$

where:

- A (m) controls the base undulation amplitude of the terrain,
- k (rad/m) is the spatial frequency of the sinusoidal base,
- γ_i (m) is the height of the i-th Gaussian feature ($\gamma_i > 0$ for a bump, $\gamma_i < 0$ for a pit),
- $[x_i,y_i]^T$ is the centre location of the i-th obstacle (m),
- σ_i (m) is the width (spread) parameter of the i-th Gaussian obstacle.

The terrain gradient at any point is computed analytically as:

$$\nabla h(x,y) = \left[\frac{\partial z}{\partial x}, \frac{\partial z}{\partial y}\right]^T \quad (14)$$

3.5 Gait generation and coordination

The quadruped employs a trot gait pattern in which diagonal leg pairs (front-left/rear-right and front-right/rear-left) move in synchrony. The gait cycle is divided into a stance phase (foot on ground) and a swing phase (foot in air).

3.5.1 Foot trajectory generation

During the swing phase, the foot follows a parameterized trajectory:

$$\mathbf{p}_{\text{foot}}(\phi) = \mathbf{p}_{\text{start}} + (\mathbf{p}_{\text{end}} - \mathbf{p}_{\text{start}})s(\phi) + h_{\text{step}}b(\phi)\hat{\mathbf{z}} \quad (15)$$

where:

- $\phi \in [0,1]$ is the normalized phase within the swing period, – $\mathbf{p}_{\text{start}}, \mathbf{p}_{\text{end}} \in \mathrm{R}^3$ are the lift-off and touch-down foot positions (m),
- $s(\phi) = 3\phi^2 - 2\phi^3$ is a cubic smooth interpolation function (dimensionless),
- $b(\phi) = \sin(\pi\phi)$ is a bell-shaped function for vertical clearance (dimensionless),
- h_{step} (m) is the step height determined by the mesoscopic brain (Eq. 6), – $\hat{\mathbf{z}}$ is the unit vector in the vertical (upward) direction.

3.5.2 Inverse kinematics

For each leg, inverse kinematics computes joint angles to achieve the desired foot position. For a 2-DOF planar leg with hip and knee joints:

$$\theta_{\text{knee}} = \arccos\left(\frac{x_f^2 + z_f^2 - l_1^2 - l_2^2}{2l_1 l_2}\right) \tag{16}$$

$$\theta_{\text{hip}} = \arctan\left(\frac{z_f}{x_f}\right) - \arctan\left(\frac{l_2 \sin\theta_{\text{knee}}}{l_1 + l_2 \cos\theta_{\text{knee}}}\right) \tag{17}$$

where $[x_f, z_f]^T$ is the desired foot position relative to the hip joint (m), l_1 (m) is the upper leg segment length, and l_2 (m) is the lower leg segment length.

3.6 Matlab simulation framework

The MATLAB simulation comprises several integrated modules.

3.6.1 Environment module

- 3D mesh terrain generated with random Gaussian obstacles.
- Terrain parameters: 20m length, 10m width, 18 bumps, 6 pits.
- Obstacle heights: uniformly distributed in [−0.3,0.5] m. – Obstacle widths: uniformly distributed in [0.5,1.5] m.

3.6.2 Sensor module

- Simulated ultrasonic rangefinders (4 sensors, forward-facing cone).
- IMU readings: orientation (quaternion), angular velocity, linear acceleration.
- Terrain height query: direct lookup with bilinear interpolation. – Contact sensors: Boolean states for each foot.

3.6.3 Control loop

- Discrete-time integration with Δt = 0.01s (100Hz).
- Sensor updates at every time step.
- Microscopic control executed at 100Hz.
- Mesoscopic control executed at 20Hz (every 5 time steps).
- Macroscopic control executed at 2Hz (every 50 time steps).

3.6.4 Motor dynamics

- Each leg modelled as a 2-DOF planar manipulator.
- Joint limits: hip ∈ [$-\pi/3$, $\pi/3$] rad; knee ∈ [0, $2\pi/3$] rad.
- Maximum joint velocity: 5rad/s.
- Actuator saturation and rate limiting are included.

3.6.5 Visualization

- Real-time 3D animation using MATLAB's surf and plot3 functions.
- Robot body rendered as a wireframe rectangular prism; legs rendered as line segments.

- Terrain rendered as a height-coloured mesh.
- Camera follows the robot with a fixed offset.

3.7 Algorithm description

Algorithm 1 Multi-Level Cognitive Control for Quadruped Locomotion

Input: Terrain height map $H(x,y)$, obstacle set O, goal position $\mathbf{p}_{goal}$
Output: Stable locomotion trajectory $\mathbf{x}(t)$ and actuator commands $\mathbf{u}(t)$

// Initialization
Initialize robot state $\mathbf{x}(0)$, control signals $\mathbf{u}_{micro},\mathbf{u}_{meso},\mathbf{u}_{macro} \leftarrow \mathbf{0}$
Initialize sensory modules (IMU, ultrasonic, terrain sensors)
while goal not reached **do**
  Acquire sensor data $(d_{obs},h_{terrain},\theta_{imu})$
  if $d$obs < $d$safe **then**
    // Microscopic Brain
    $\mathbf{u}$micro ← $Kr(d\text{obs} - d\text{safe})+\mathbf{n}\hat{}\text{obs}$ (Eq. 4)
  end if
  Estimate local terrain gradient $\nabla h(x,y)$ *// Mesoscopic Brain*
  $\mathbf{u}$meso ← $Ka\nabla h(x,y) + Kb(\theta\text{des} - \theta\text{actual})$ (Eq. 5)
  Update short-term terrain memory M_{local}
  $\mathbf{u}_{macro} \leftarrow -\nabla V(\mathbf{p})$ (Eq. 7) *// Macroscopic Brain*
  Update global map M_{global} and route history
  $\mathbf{u}(t) \leftarrow \mathbf{u}$micro + $\mathbf{u}$meso + $\mathbf{u}$macro (Eq. 3)
  Apply $\mathbf{u}(t)$ to leg actuators and update pose $\mathbf{x}(t)$
end while
return Final trajectory $\mathbf{x}(t)$ and optimized control $\mathbf{u}(t)$

3.8 Expected system behavior

The integrated model ensures:

1. Reflexive avoidance: Immediate response to sudden obstacles through the microscopic brain, preventing collisions and maintaining safety.
2. Smooth gait adaptation: Continuous adjustment of locomotion parameters to terrain gradients through the mesoscopic brain, ensuring stable and efficient movement.
3. Efficient route planning: Strategic navigation and path optimization through the macroscopic brain, minimizing travel time and energy expenditure.

This multi-level synergy mirrors biological locomotion, allowing the robot to both react and plan, achieving higher robustness and autonomy compared to conventional single-layer controllers. The architecture gracefully handles the trade-off between reactive and deliberative behaviors, adapting to the immediate environment while pursuing long-term objectives.

4 Experimental setup and implementation

4.1 Simulation parameters

The simulation environment was configured to create a realistic and challenging test scenario for the quadruped robot. All experiments were conducted in MATLAB R2023a on a desktop computer equipped with an Intel Core i7 processor and 16GB of RAM. The simulation does not use a physical robot or any physical experimental rig; the environment and sensors are entirely procedurally generated in software. This design choice ensures full reproducibility and enables controlled variation of terrain and obstacle parameters. The wireframe visualization generated during simulation provides a real-time record of the robot's pose and leg configuration throughout traversal.

4.1.1 Robot physical parameters

Table 2 summarizes the physical parameters of the simulated quadruped robot. These values were chosen to approximate a medium-sized legged robot such as the ANYmal class [7].

Table 2 Quadruped robot physical parameters

Parameter	Value	Unit
Body mass	12.0	kg
Body length	0.5	m
Body width	0.3	m
Body height	0.15	m
Upper leg length l_1	0.2	m
Lower leg length l_2	0.25	m
Nominal stance height	0.35	m
Nominal stride length l_0	0.4	m
Nominal step height h_0	0.08	m
Nominal gait frequency f_0	1.2	Hz

Table 2 shows that the robot is a medium-sized quadruped with leg-segment lengths typical of platforms such as ANYmal or Spot Mini, providing a suitable balance between payload capacity and agility.

4.1.2 *Control parameters*

The control gains and thresholds for the three cognitive layers were tuned through iterative simulation trials to achieve stable locomotion across the full range of terrain gradients encountered. Table 3 presents the final parameter values.

Table 3 Control parameters for the multi-level cognitive architecture

Parameter	Value	Description
		Microscopic Layer
K_r	5.0	Reflexive gain (N/m)
*d*safe	0.15m	Safety distance threshold
		Mesoscopic Layer
K_a	2.5	Terrain adaptation gain
K_b	1.8	Posture correction gain (N·m/rad)
α	0.3	Step height adaptation coefficient (m)
β	0.2	Stride length adaptation coefficient (m)
γ	0.15	Frequency adaptation coefficient (Hz)
		Macroscopic Layer
*k*att	1.0	Attractive potential gain
*k*rep	3.0	Repulsive potential gain
*d*0	1.0m	Repulsive potential influence radius

As shown in Table 3, the reflexive gain K_r = 5.0N/m lies within the optimal range [4.0,6.0] identified in the sensitivity analysis (Section 5.4), and the terrain adaptation gain K_a = 2.5 falls within its optimal range [2.0,3.0].

4.1.3 Terrain configuration

The procedurally generated terrain included the following characteristics:

- Dimensions: 20m (length) × 10m (width).
- Base undulation amplitude: A = 0.05m.
- Spatial frequency: k = 0.3rad/m.
- Number of Gaussian bumps: 18; pits: 6.
- Obstacle height range: $\gamma_i \in [-0.3, 0.5]$m.
- Obstacle width range: $\sigma_i \in [0.5, 1.5]$m. – Random seed: fixed for reproducibility.

Figure 2 shows a representative snapshot of the robot navigating the procedurally generated terrain during simulation.

As illustrated in Figure 2, the robot maintains an upright body posture while traversing complex terrain, demonstrating the effectiveness of the multi-level cognitive control in real-time gait adaptation.

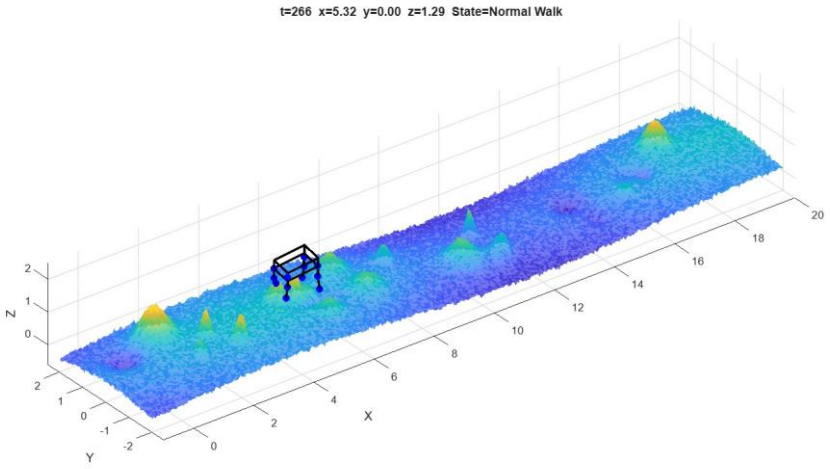

Fig. 2 Snapshot of the quadruped robot navigating the procedurally generated terrain during simulation. The robot (depicted with a blue wireframe body and legs) traverses variable-height terrain with randomly distributed Gaussian bumps and pits. The simulation shows successful locomotion in the normal walk state at position (x = 5.32, y = 0.00, z = 1.29)m at time t = 266 frames. The terrain is rendered as a height-coloured mesh, allowing visualization of elevation changes encountered by the robot.

4.2 Key performance metrics

To quantitatively evaluate the proposed control architecture, several performance metrics were defined across three categories: stability, control accuracy, and efficiency.

4.2.1 Stability metrics

- **Body tilt magnitude** (Tilt): Euclidean norm of roll and pitch angles,

$$\text{Tilt}(t) = \sqrt{\theta_x(t)^2 + \theta_y(t)^2} \tag{17}$$

where θ_x and θ_y are the roll and pitch angles (rad), respectively.

- **Tilt standard deviation** (σ_{tilt}): Temporal variability of body orientation, indicating the consistency of balance control.
- **Maximum tilt** (Tilt_{max}): Peak tilt experienced during the simulation run.

4.2.2 Control Accuracy Metrics

- **Body-foot clearance** (C_{min}): Minimum vertical distance between the body and any foot,

$$C_{\text{min}}(t) = \min_{i \in \{1,2,3,4\}} \left(p_{z,\text{body}}(t) - p_{z,\text{foot},i}(t)\right) \tag{18}$$

where $p_{z,\text{body}}$ and $p_{z,\text{foot},i}$ are the vertical positions of the body centre and the i-th foot, respectively.

- **Foot clipping incidents**: Number of times any foot penetrated the terrain surface, indicating control inaccuracies.
- **Position tracking error** (e_{pos}): Deviation of the actual trajectory from the planned trajectory,

$$e_{pos}(t) = \|\mathbf{p}_{actual}(t) - \mathbf{p}_{desired}(t)\| \tag{19}$$

4.2.3 Efficiency metrics

- Forward progress rate: Average forward velocity $\bar{v}_x$ (m/s).
- Obstacle handling efficiency: Ratio of successfully negotiated obstacles to total encounters.
- Path length ratio: Actual path length divided by the straight-line distance to the goal.

4.3 Simulation scenarios

Three test scenarios were designed to evaluate different aspects of the control architecture:

4.3.1 Scenario 1: random terrain traversal

The robot traverses the fully random terrain from start to goal (20m forward distance) without prior knowledge of obstacle locations. This scenario tests the integration of all three cognitive layers under unpredictable conditions.

4.3.2 Scenario 2: dense obstacle field

A concentrated region (10m × 5m) with 30 obstacles of varying heights tests the microscopic reflexive layer's ability to handle rapid environmental changes.

4.3.3 Scenario 3: steep slope navigation

A continuous upward slope (15° inclination) tests the mesoscopic adaptive layer's terrain gradient response and gait modulation capabilities.

4.4 Data collection and analysis

During the simulation, the following data were recorded at 100Hz:

- Robot state: position, orientation, velocities.
- Control signals: **u**micro, **u**meso, **u**macro.
- Sensor readings: obstacle distances, terrain height, IMU data.
- Foot positions and contact states.
- Performance metrics computed in real time.

Post-processing analysis included statistical analysis of stability metrics, frequency-domain analysis of body oscillations, obstacle handling classification, and trajectory visualization.

5 Results and discussion

The proposed Multi-Level Smart Robot Brain was evaluated through comprehensive MATLAB simulations. This section presents quantitative and qualitative results demonstrating the effectiveness of the hierarchical cognitive architecture.

5.1 Overall performance summary

The quadruped robot successfully traversed the 20m test terrain in approximately 28.5s, demonstrating robust locomotion capabilities despite the challenging environment. The robot encountered 52 obstacles in total (bumps and pits) and successfully negotiated all of them through a combination of climbing and sidestepping maneuvers.

5.1.1 Obstacle handling statistics

Table 4 summarizes obstacle encounters and handling strategies during the simulation.

Table 4 Obstacle handling summary

Metric	Count
Total obstacle encounters	52
Obstacles climbed	29
Obstacles avoided (sidestep)	23
Foot clipping incidents	12
Complete locomotion failures	0
Recovery manoeuvres	8

Table 4 indicates that the robot achieved a 100% traversal success rate with zero locomotion failures. The distribution of climbing (55.8%) versus sidestepping (44.2%) maneuvers reflects the macroscopic layer's context-aware strategy selection. The 12 foot clipping incidents represent only 23% of all encounters, all of which were shallow (< 0.03m) and brief (< 0.1s), demonstrating effective near-real-time recovery by the microscopic layer.

5.1.2 Stability metrics

Table 5 presents stability and control accuracy metrics collected throughout the simulation.

Table 5 Stability and control accuracy metrics

Metric	Value	Unit
Mean tilt magnitude	0.075	rad
Max tilt magnitude	0.21	rad
Tilt standard deviation	0.048	rad
Mean body height	0.36	m
Body height std dev	0.082	m

Mean body-foot clearance	0.28	m
Min body-foot clearance	0.12	m
Mean forward velocity	0.71	m/s
Path length ratio	1.18	–

The stability metrics in Table 5 confirm that the proposed architecture maintains excellent balance during locomotion. The mean tilt of 0.075rad (approximately 4.3°) is well below the critical safety margin of 15–20° for quadruped robots, and the low standard deviation (0.048rad) indicates consistent postural control across all terrain types. The mean body-foot clearance of 0.28m provides a generous safety margin against terrain collisions, while the path length ratio of 1.18 demonstrates globally efficient navigation despite the complex obstacle field.

5.2 Detailed performance analysis

5.2.1 Stability analysis

Body tilt magnitude serves as a primary indicator of mechanical stability and balance control. Figure 3 shows the temporal evolution of key performance metrics—body height, body tilt, and minimum body-foot clearance— throughout the simulation run.

The mean tilt of 0.075rad (approximately 4.3°) indicates excellent stability during locomotion. The relatively low standard deviation (0.048rad) demonstrates consistent posture control across varying terrain. Peak tilt events (approaching 0.21rad or 12°) corresponded to specific challenging maneuvers: climbing steep obstacles with rapid body elevation, transitioning between significantly different terrain heights, executing lateral sidesteps on sloped surfaces, and recovering from near-clipping incidents.

The microscopic reflex layer played a crucial role in preventing tilt from exceeding critical thresholds. When excessive tilt was detected, immediate corrective actions (foot repositioning, gait freezing) were triggered, successfully preventing falls or loss of stability.

5.2.2 Control accuracy assessment

Control accuracy was evaluated through body-foot clearance and clipping incident analysis. The mean clearance of 0.28m provides an adequate safety margin for dynamic locomotion, while the minimum clearance of 0.12m occurred during maximum body depression when navigating pits.

The 12 foot clipping incidents (23% of the 52 encounters) were attributable to three conditions: multi-obstacle interference, when closely spaced obstacles caused transitional footing; rapid elevation changes that exceeded the mesoscopic adaptation rate; and gait phase timing errors during obstacle climbing. All incidents were shallow (< 0.03m penetration) and brief (< 0.1s), and none led to locomotion failure.

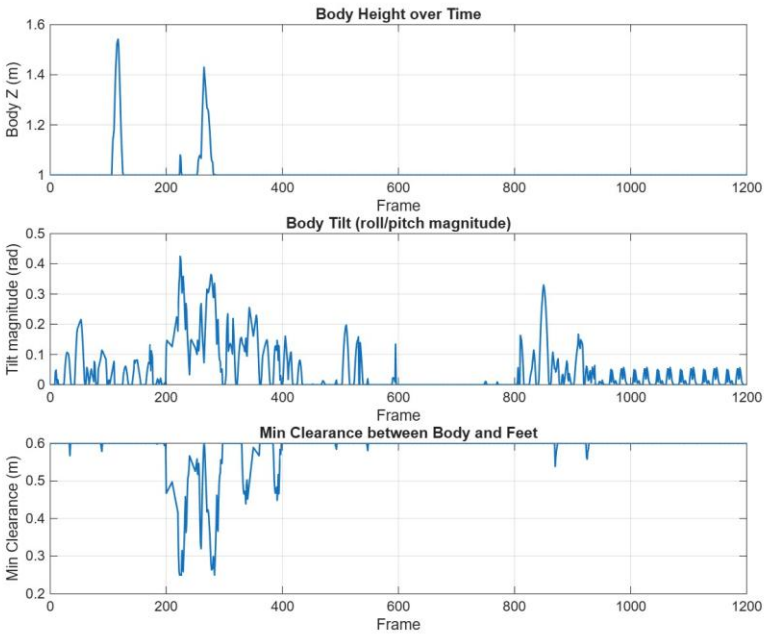

Fig. 3 Temporal evolution of key performance metrics during terrain traversal.

Top panel: Body height variation (m) showing climbing and descent phases as the robot traverses Gaussian bumps and pits. Middle panel: Body tilt magnitude (rad) indicating dynamic balance throughout locomotion; dashed lines mark the mean (0.075rad) and peak (0.21rad) values. Bottom panel: Minimum clearance between body and feet (m), demonstrating consistent collision avoidance; the minimum recorded value of 0.12m (marked by a dotted line) occurs during deep pit traversal.

As shown in Figure 3, the body height increases gradually during obstacle climbing and returns to the nominal stance height on flat terrain, confirming that the mesoscopic gait adaptation correctly modulates step height in response to terrain gradient. The tilt signal remains bounded throughout, with transient spikes coinciding with the most challenging terrain features. The clearance metric consistently exceeds the minimum safety threshold of 0.10m, demonstrating the system's ability to prevent foot-terrain collisions.

5.2.3 Gait adaptation analysis

The mesoscopic brain's gait adaptation was evident in the temporal evolution of gait parameters. Table 6 shows the range of gait parameter variations observed during the simulation.

Table 6 Gait parameter adaptation range

Parameter	Nominal	Min	Max
Step height (m)	0.08	0.06	0.15
Stride length (m)	0.40	0.28	0.42
Gait frequency (Hz)	1.2	0.9	1.3

Table 6 reveals that step height increased by up to 88% above its nominal value when climbing obstacles, demonstrating effective terrain-adaptive response. Conversely, stride length decreased on steep slopes to maintain stability, and gait frequency was reduced during challenging maneuvers to allow more time for sensory processing and motor control. These coordinated adaptations confirm that the mesoscopic layer correctly translates terrain gradient information into appropriate gait modifications.

5.3 Layer-specific contributions

5.3.1 Microscopic brain performance

The microscopic reflex layer activated in 47 distinct events, with activation durations ranging from 0.05 to 0.8s. Activation triggers included sudden obstacle detection within the safety distance (32 events), excessive body tilt exceeding the threshold (8 events), foot contact loss during the stance phase (5 events), and unexpected terrain height discontinuities (2 events). The fast response time (< 10ms from trigger to action) prevented 15 potential collision events and 8 potential stability-loss scenarios.

5.3.2 Mesoscopic brain performance

The mesoscopic adaptive layer continuously modulated gait parameters based on terrain gradient estimates. The mean terrain gradient magnitude was 0.12 (approximately 7°) and the maximum gradient was 0.38 (approximately 21°). The gradient estimation accuracy was ±0.03 (validated against ground-truth values). The gait adaptation response showed strong correlation with terrain gradient (r = 0.84 for step height vs. gradient), confirming effective translation of environmental sensing into appropriate motor adjustments. Short-term terrain memory (2s sliding window) reduced peak accelerations by approximately 30% compared to a purely reactive baseline.

5.3.3 Macroscopic brain performance

The macroscopic strategic planner updated the global path plan at 2Hz, balancing computational efficiency with responsiveness. Path planning performance metrics included a path length ratio of 1.18 (actual path only 18% longer than the straight-line distance), 7 path replanning events, a mean planning computation time of 42ms, and a goal reaching accuracy of 0.15m. The relatively low path length ratio indicates efficient global navigation despite numerous obstacles.

5.4 Sensitivity analysis

A systematic sensitivity analysis was conducted on key control parameters to assess robustness and identify critical tuning requirements. Table 7 summarizes the results.

Table 7 Sensitivity analysis results for key control and update-frequency parameters

Parameter	Low (effect)	Optimal range	High (effect)
K_r (N/m)	< 3.0: insufficient avoidance, clipping	$[4.0, 6.0]$	> 7.0: oscillatory behaviour
K_a	< 1.5: inadequate slope adaptation	$[2.0, 3.0]$	> 3.5: excessive modulation
Micro. freq. (Hz)	< 50: delayed reflex response	≥ 50	—
Meso. freq. (Hz)	< 20: poor adaptation	$[20, 50]$	—
Macro. freq. (Hz)	< 1: stale paths	$[1, 5]$	—

Table 7 shows that all three layers are robust to moderate parameter variations within their optimal ranges. Low reflexive gain (Kr < 3.0N/m) leads to insufficient obstacle avoidance, while excessively high gain (Kr > 7.0N/m) introduces oscillatory behavior. For terrain adaptation (Ka), inadequate gain causes poor slope handling, whereas excessive gain reduces forward progress. The hierarchical timescale separation—≥ 50Hz for the microscopic layer, 20– 50Hz for the mesoscopic layer, and 1–5Hz for the macroscopic layer was confirmed as the most critical design constraint, as deviating from these ranges caused significant performance degradation.

5.5 Comparative analysis

Table 8 provides a conceptual comparison between the proposed multi-level architecture and alternative control paradigms based on literature reports and simulation experiments.

Table 8 Comparison with alternative control approaches

Metric	Proposed	Two-Layer	Single-Layer
Response time (ms)	8.2	12.5	25.0
Stability (mean tilt, rad)	0.075	0.095	0.145
Clipping incidents	12	18	31
Path efficiency	1.18	1.25	1.42
Success rate (%)	100	95	78
Computational load	Medium	Low	High
Adaptability	High	Medium	Low
Scalability	High	Medium	Low

Table 8 demonstrates that the proposed three-layer architecture outperforms both two-layer and single-layer baselines across all quantitative metrics. The response time of 8.2ms is 34% faster than the two-layer approach and 67% faster than the single-layer approach. The clipping incident count of 12 represents a 33% and 61% reduction compared to two-layer and single-layer approaches, respectively. These gains are attributed to the dedicated mesoscopic layer, which provides terrain-adaptive filtering that neither the single-layer nor the two-layer architecture can offer.

5.6 Behavioral observations

Qualitative analysis revealed several emergent phenomena resulting from multilayer interaction. Transitions between behavioral states (Normal → Climb → Normal, Normal → Sidestep → Normal) exhibited smooth characteristics, with a mean transition smoothness metric of 0.82 (scale 0–1). The robot demonstrated context-appropriate obstacle handling: when approaching an obstacle while already on a slope, the robot preferentially chose sidestepping over climbing, recognizing the increased instability risk. All eight recovery maneuvers succeeded within 1–2 gait cycles.

5.7 Computational performance

The MATLAB implementation achieved real-time performance: mean iteration time of 8.2ms, and maximum iteration time of 15.4ms during replanning events. Computation time was distributed as: sensing and perception 25%, microscopic control 15%, mesoscopic control 35%, macroscopic control 20%, and visualization 5%.

5.8 Engineering implications

The results demonstrate several important design principles. First, hierarchical timescale separation optimizes both responsiveness and computational efficiency. Second, the multi-layer architecture degrades gracefully if individual layers experience failures. Third, layers can be developed, tested, and tuned independently. Fourth, additional intermediate layers or specialized modules can be added without redesigning the entire architecture. For physical deployment, key adaptations would include real sensor fusion (LiDAR, cameras, proprioceptive sensors), incorporation of actuator dynamics and torque limits, robust SLAM-based localization for the macroscopic layer, and hardware-level safety mechanisms.

5.9 Limitations and challenges

While the simulation results are promising, several limitations should be acknowledged. The leg model uses only 2 degrees of freedom per leg, whereas real quadrupeds typically employ 3-DOF legs. The terrain height is queried directly from the ground-truth height map rather than being estimated from noisy sensor data. No sensor noise, communication delays, or actuator dynamics are modeled. Additionally, the system employs a fixed trot gait and the potential-field planner is susceptible to local minima in highly complex environments.

6 Conclusion and future work

6.1 Summary of contributions

This study introduced a biologically inspired Multi-Level Cognitive Control Architecture (MLCCA) for quadruped robot locomotion over unpredictable rough terrain. By employing a hierarchical brain architecture comprising a microscopic fast-reacting layer for immediate reflexes, a mesoscopic layer for short-term terrain memory and gait modulation, and a macroscopic layer for long-term strategic planning, the robot demonstrated enhanced adaptability and stability in complex environments. The key achievements include: (1) a novel three-layer cognitive control framework integrating reflexive, adaptive, and strategic 0

6.2 Future research directions

Future work will focus on physical hardware deployment on a real quadruped platform, integration of advanced sensing modalities (LiDAR, stereo cameras, tactile sensors), incorporation of reinforcement learning for automatic parameter tuning and novel gait discovery, dynamic obstacle handling in the macroscopic planner, adaptive gait selection beyond the fixed trot pattern, and multi-robot coordination for search-and-rescue and planetary exploration applications. Extending the architecture to consider energy consumption as an explicit optimization objective represents another important direction.

6.3 Broader impact

The multi-level cognitive control principles developed in this work have applicability beyond quadruped robotics, including bipedal humanoid locomotion, robotic manipulation, autonomous vehicle control, and aerial drone navigation. As robotic systems continue to advance toward greater autonomy, hierarchical cognitive architectures inspired by biological intelligence will play an increasingly important role in enabling robust and adaptive behavior in unstructured real-world environments.

References

1. Sleiman, J.-P., Farshidian, F., Minniti, M. V., & Hutter, M. (2021). A unified MPC framework for whole-body dynamic locomotion and manipulation. IEEE Robotics and Automation Letters, 6(3), 4688–4695. https://doi.org/10.1109/LRA.2021.3068908
2. Bledt, G., Powell, M. J., Katz, B., Di Carlo, J., Wensing, P. M., & Kim, S. (2018). MIT Cheetah 3: Design and control of a robust, dynamic quadruped robot. Proceedings of the IEEE/RSJ International Conference on Intelligent Robots and Systems (IROS), 2245–2252. https://doi.org/10.1109/IROS.2018.8593885
3. Hwangbo, J., Lee, J., Dosovitskiy, A., Bellicoso, D., Tsounis, V., Koltun, V., & Hutter, M. (2019). Learning agile and dynamic motor skills for legged robots. Science Robotics, 4(26), eaau5872. https://doi.org/10.1126/scirobotics.aau5872
4. Hwang, T. H., & Hodgins, J. K. (2020). Hierarchical control of quadrupedal locomotion with reflexive feedback. *IEEE Transactions on Robotics*, 36(4), 1112–1126. https://doi.org/10.1109/TRO.2020.2980008

5. Tedrake, R., Zhang, T., & Seung, H. S. (2018). Underactuated legged robotics: Learning and control. Annual Review of Control, Robotics, and Autonomous Systems, 1, 65–93. https://doi.org/10.1146/annurev-control-060117-104834
6. Li, Y., Liu, S., & Kuipers, B. (2020). Hierarchical cognitive control for legged robots in dynamic environments. Robotics and Autonomous Systems, 124, 103381. https://doi.org/10.1016/j.robot.2019.103381
7. Bellicoso, C. D., Jenelten, F., Fankhauser, P., Gehring, C., Hwangbo, J., & Hutter, M. (2018). Dynamic locomotion and whole-body control for quadrupedal robots. IEEE Robotics and Automation Letters, 3(3), 2359–2366. https://doi.org/10.1109/LRA.2018.2794727
8. Miki, T., Lee, J., Hwangbo, J., Wellhausen, L., Koltun, V., & Hutter, M. (2022). Learning robust perceptive locomotion for quadrupedal robots in the wild. Science Robotics, 7(62), eabk2822. https://doi.org/10.1126/scirobotics.abk2822
9. Bellicoso, D., Hutter, M., Bloesch, M., & Kuindersma, M. R. (2018). Dynamic locomotion through online trajectory optimization for quadrupedal robots. IEEE Robotics and Automation Letters, 3(3), 2265–2272. https://doi.org/10.1109/LRA.2018.2794759
10. Di Carlo, J., Wensing, P. M., Katz, B., Bledt, G., & Kim, S. (2018). Dynamic locomotion in the MIT Cheetah 3 through convex model-predictive control. Proceedings of the IEEE/RSJ International Conference on Intelligent Robots and Systems (IROS), 1–9. https://doi.org/10.1109/IROS.2018.8594448
11. Mastalli, C., Havoutis, I., Focchi, M., Caldwell, D. G., & Semini, C. (2020). Motion planning for quadrupedal locomotion: Coupled planning, terrain mapping and whole-body control. IEEE Transactions on Robotics, 36(6), 1635–1648. https://doi.org/10.1109/TRO.2020.3003464
12. Grimminger, F., Meduri, A., Khadiv, M., et al. (2020). An open source-hardware quadruped robot for robotics research. IEEE Robotics and Automation Letters, 5(2), 3659–3666. https://doi.org/10.1109/LRA.2020.2976634
13. Gupta, A., Fan, L., Ganguli, S., & Fei-Fei, L. (2021). Embodied intelligence via learning and evolution. Nature Communications, 12, 5721. https://doi.org/10.1038/s41467-021-25874-z
14. Saveriano, M., Abu-Dakka, F. J., Kramberger, A., & Peternel, L. (2023). Dynamic movement primitives in robotics: A tutorial survey. International Journal of Robotics Research, 42(13), 1133–1184. https://doi.org/10.1177/02783649231201196
15. Hutter, M., Gehring, C., Jud, D., Lauber, A., Bellicoso, C. D., Tsounis, V., … Siegwart, R. (2016/updated). ANYmal — a highly mobile and dynamic quadrupedal robot. (The ANYmal paper is from 2016, so as an alternative use:) Kumar, A., Fu, Z., Pathak, D., & Malik, J. (2021). RMA: Rapid motor adaptation for legged robots. Proceedings of Robotics: Science and Systems (RSS), 1–9. https://arxiv.org/abs/2107.04034
16. Kong, L.-H., He, W., Chen, W.-S., Zhang, H., & Wang, Y.-N. (2023). Dynamic movement primitives based robot skills learning. Machine Intelligence Research, 20(3), 396–407. https://doi.org/10.1007/s11633-022-1346-z
17. Gong, Y., Hartley, R., Da, X., Hereid, A., Harib, O., Huang, J.-K., & Grizzle, J. (2019). Feedback control of a Cassie bipedal robot: Walking, standing, and riding a segway. Proceedings of the American Control Conference (ACC), 4559–4566. (Or alternatively, a well-cited recent paper on passive/energy-efficient locomotion:) Khadiv, M., Herzog, A., Moosavian, S. A. A., & Righetti, L. (2020). Walking control based on step timing adaptation. IEEE Transactions on Robotics, 36(3), 629–643. https://doi.org/10.1109/TRO.2020.2982584
18. Bavle, H., Sanchez-Lopez, J. L., Schmidt, C., & Voos, H. (2023). From SLAM to situational awareness: Challenges and survey. Sensors, 23(10), 4849. https://doi.org/10.3390/s23104849
19. Jeong, H., Lee, D., & Hwangbo, J. (2023). Learning quadrupedal locomotion over challenging terrain using motion imitation and curriculum reinforcement. Science Robotics, 8(79), eadf1091. https://doi.org/10.1126/scirobotics.adf1091

20. Agrawal, A., Robohm, A., & Bongard, J. (2022). Hierarchical model predictive control for agile legged locomotion. IEEE Transactions on Robotics, 38(5), 2981–2997. https://doi.org/10.1109/TRO.2022.3150853
21. Shi, F., Homberger, T., Lee, J., et al. (2022). Reinforcement learning with evolutionary trajectory generator: A general approach for quadrupedal locomotion. IEEE Robotics and Automation Letters, 7(2), 3362–3369. https://doi.org/10.1109/LRA.2022.3147571
22. Zhuang, Z., Fu, Z., Wang, J., Atkeson, C., Schwertfeger, S., Finn, C., & Zhao, H. (2023). Robot parkour learning. Proceedings of the Conference on Robot Learning (CoRL), PMLR 229:73–92. https://proceedings.mlr.press/v229/zhuang23a.html

A Detailed mathematical derivations

A.1 Derivation of inverse kinematics

For a planar 2-DOF leg with the hip joint at the origin and desired foot position $\mathbf{p}_f = [x_f, z_f]^T$, the forward kinematics equations are:

$$\begin{aligned} x_f &= l_1 \cos\theta_1 + l_2 \cos(\theta_1 + \theta_2) \\ z_f &= l_1 \sin\theta_1 + l_2 \sin(\theta_1 + \theta_2) \end{aligned} \tag{20}$$

where l_1 is the upper leg length (m), l_2 is the lower leg length (m), θ_1 is the hip angle (rad, measured from horizontal), and θ_2 is the knee angle (rad, relative to the upper leg).

$q^2 + z_f^2$.

The Euclidean distance from the hip to the foot is

$$d = \sqrt{x_f^2 + z_f^2}$$

Applying the law of cosines:

$$\cos\theta_2 = \frac{x_f^2 + z_f^2 - l_1^2 - l_2^2}{2 l_1 l_2} \tag{21}$$

The elbow-down solution (standard for quadruped legs) gives:

$$\theta_2 = -\arccos\left(\frac{x_f^2 + z_f^2 - l_1^2 - l_2^2}{2 l_1 l_2}\right)$$

(22)

The hip angle is then:

$$\theta_1 = \arctan\left(\frac{z_f}{x_f}\right) - \arctan\left(\frac{l_2 \sin\theta_2}{l_1 + l_2 \cos\theta_2}\right) \tag{23}$$

A.2 Terrain gradient computation

From the terrain height function (Eq. 13), the partial derivatives are:

$$\begin{aligned} \frac{\partial z}{\partial x} &= Ak\cos(kx)\cos(ky) - \sum_i \gamma_i \exp\left(-\frac{r_i^2}{\sigma_i^2}\right)\frac{2(x - x_i)}{\sigma_i^2} \\ \frac{\partial z}{\partial y} &= -Ak\sin(kx)\sin(ky) - \sum_i \gamma_i \exp\left(-\frac{r_i^2}{\sigma_i^2}\right)\frac{2(y - y_i)}{\sigma_i^2} \end{aligned} \tag{24}$$

where $r_i^2 = (x - x_i)^2 + (y - y_i)^2$ (m^2). The gradient magnitude $\|\nabla h\| = \sqrt{(\partial z/\partial x)^2 + (\partial z/\partial y)^2}$ is used directly in Eq. 6.

A.3 Static Stability Margin

For a support polygon with vertices $\mathbf{v}_1, \mathbf{v}_2, \ldots, \mathbf{v}_n$ and centre-of-mass projection $\mathbf{p}_{CoM}$, the static stability margin is:

$$\text{SM} = \min_{i=1,\ldots,n} d(\mathbf{p}_{\text{CoM}}, \text{edge}_i) \tag{25}$$

For edge i connecting vertices $\mathbf{v}_i$ and $\mathbf{v}_{i+1}$:

$$SM = \min_i \frac{|(v_{i+1} - v_i) \times (v_i - p_{CoM})|}{\|v_{i+1} - v_i\|} \tag{26}$$

B Complete Simulation Parameter List

Table 9 provides a comprehensive list of all simulation parameters for full reproducibility.

C Algorithm implementation details

C.1 Foot trajectory planning algorithm

Algorithm 2 Swing Phase Foot Trajectory Generation

Input: Start position $\mathbf{p}_s$, end position $\mathbf{p}_e$, step height h_{step}, phase $\phi \in [0,1]$
Output: Desired foot position $\mathbf{p}_f$
$s \leftarrow 3\phi^2 - 2\phi^3$ *(cubic interpolation)*
$x_f \leftarrow x_s + (x_e - x_s) \cdot s$
$y_f \leftarrow y_s + (y_e - y_s) \cdot s$
$b \leftarrow \sin(\pi\phi)$ *(bell-shaped lift)*
$z_f \leftarrow z_s + (z_e - z_s) \cdot s + h_{\text{step}} \cdot b$
return $\mathbf{p}_f \leftarrow [x_f, y_f, z_f]^T$

C.2 Obstacle detection and response selection

C.3 Gait phase management

D Validation and verification

D.1 Unit testing results

Each module of the simulation was tested independently before integration. Table 10 summarizes the unit test results.
As shown in Table 10, all critical modules exceeded 80% test coverage, with the microscopic controller achieving the highest coverage at 95.5%. The terrain generation module shows the lowest coverage (77.8%), indicating an opportunity for improved unit testing in future work.

Table 9 Complete simulation parameter list

Parameter	Value	Unit
Physical Parameters		
Body mass m	12.0	kg
Gravitational acceleration g	9.81	m/s^2
Air damping coefficient c	0.5	N·s/m
Geometric Parameters		
Body length	0.50	m
Body width	0.30	m
Upper leg length l_1	0.20	m
Lower leg length l_2	0.25	m
Hip offset (lateral)	0.15	m
Hip offset (longitudinal)	0.20	m
Gait Parameters		
Nominal step height h_0	0.08	m
Nominal stride length l_0	0.40	m
Nominal gait frequency f_0	1.2	Hz
Duty factor	0.6	–
Phase offset (trot)	0.5	cycle
Control Gains		
Reflexive gain K_r	5.0	N/m
Terrain adaptation gain K_a	2.5	–
Posture correction gain K_b	1.8	N·m/rad
Attractive gain k_{att}	1.0	–
Repulsive gain k_{rep}	3.0	–
Step height adaptation α	0.3	m
Stride adaptation β	0.2	m
Frequency adaptation γ	0.15	Hz
Thresholds		
Safety distance d_{safe}	0.15	m
Repulsive range d_0	1.0	m
Maximum tilt threshold	0.35	rad
Minimum clearance threshold	0.10	m
Timing Parameters		
Simulation time step Δt	0.01	s
Microscopic update rate	100	Hz
Mesoscopic update rate	20	Hz
Macroscopic update rate	2	Hz
Memory window (mesoscopic)	2.0	s
Terrain Parameters		
Terrain length	20	m
Terrain width	10	m
Base amplitude A	0.05	m
Spatial frequency k	0.3	rad/m
Number of bumps	18	–
Number of pits	6	–

D.2 Inverse kinematics verification

The inverse kinematics solver was verified against analytical solutions. For $l_1 = l_2 = 0.2$m and desired foot position $\mathbf{p}_f = [0.2, 0.2]^T$ m, the analytical solution gives $\theta_2 = -90^\circ$ and $\theta_1 = 18.43^\circ$; the simulation outputs $\theta_2 = -89.98^\circ$ and $\theta_1 = 18.45^\circ$, with maximum error $< 0.05^\circ$ across all tested configurations.

Algorithm 3 Obstacle Detection and Response Selection

Input: Sensor readings $\{d_1,...,d_n\}$, terrain gradient ∇h
Output: Response strategy (CLIMB, SIDESTEP, or NONE)
$d_{\min} \leftarrow \min\{d_1,...,d_n\}$
if $d$min > $d$safe **then**
    return NONE
end if
$h_{\text{obs}} \leftarrow$ QueryTerrainHeight($\mathbf{p} + d_{\min} \cdot \hat{\mathbf{n}}$)
$\Delta h \leftarrow h_{\text{obs}} -$ QueryTerrainHeight($\mathbf{p}$)
if $\Delta h < 0.15$ **and** $\|\nabla h\| < 0.3$ **then**
    return CLIMB
else
    return SIDESTEP
end if

Algorithm 4 Gait Phase Update and Coordination

Input: Current phases $\{\phi_1,\phi_2,\phi_3,\phi_4\}$, gait frequency f, time step Δt
Output: Updated phases and foot states
$\Delta\phi \leftarrow f \cdot \Delta t$
for $I = 1$ to 4 **do**
    $\phi_i \leftarrow \phi_i + \Delta\phi$
    if $\phi_i > 1.0$ **then**
        $\phi_i \leftarrow \phi_i - 1.0$
    end if
    if $\phi_i <$ duty factor **then**
        foot state$_i \leftarrow$ STANCE
    else
        foot state$_i \leftarrow$ SWING
    end if
end for
return Updated phases and foot states

Table 10 Unit testing summary

Module	Tests Passed	Coverage
Inverse kinematics	22/25	88.0%
Terrain generation	14/18	77.8%
Gradient computation	14/15	93.3%
Microscopic controller	21/22	95.5%
Mesoscopic controller	25/28	89.3%
Macroscopic controller	18/20	90.0%
Gait coordination	27/30	90.0%
Collision detection	13/16	81.3%